C. R. Geoscience 351 (2019) 253–259

Contents lists available at ScienceDirect

Comptes Rendus Geoscience

www.sciencedirect.com

Internal Geophysics (Physics of Earth's Interior)

High-pressure generation in the Kawai-type multianvil apparatus equipped with tungsten-carbide anvils and sintered-diamond anvils, and X-ray observation on $CaSnO_3$ and $(Mg,Fe)SiO_3$

Daisuke Yamazaki [a,*], Eiji Ito [a], Takashi Yoshino [a], Noriyoshi Tsujino [a], Akira Yoneda [a], Hitoshi Gomi [a], Jaseem Vazhakuttiyakam [a], Moe Sakurai [a], Youyue Zhang [a], Yuji Higo [b], Yoshinori Tange [b]

[a] Institute for Planetary Materials, Okayama University, Tottori, Japan
[b] Japan Synchrotron Radiation Research Institute, Hyogo, Japan

ARTICLE INFO

Article history:
Received 20 March 2018
Accepted after revision 12 July 2018
Available online 10 August 2018

Handled by Robert C. Liebermann

Keywords:
Kawai-type multianvil apparatus
Sintered diamond anvil
Tungsten-carbide anvil
Pressure generation
Post-perovskite

ABSTRACT

We extended the attainable pressure of the Kawai-type multianvil apparatus to 71.3 GPa and 120.3 GPa at room temperature by equipping it with tungsten carbide (WC) and sintered diamond (SD) cubic anvils, respectively. In the experiments with WC anvils, pressure decreased largely, $\Delta P \sim -20$ GPa, on heating from room temperature to 1500 K. In the experiments with SD anvils, pressure also dropped to 105 GPa from 120 GPa at 1673 K. In order to generate higher pressure and temperatures, therefore, innovation of SD material in both quality and size are essential, together with improvements of cell assembly. Besides pressure generation, we conducted in situ energy-dispersive X-ray diffraction observations on $CaSnO_3$ and $(Mg,Fe)SiO_3$ in the experiments with WC and SD anvils, respectively. We observed the growth of new peaks, which can be assigned to the post-perovskite phase, transformed from a starting material of $CaSnO_3$ perovskite at 48.4 GPa and 1500 K, although they are not clearly identified. In contrast, we could not observe the post-perovskite phase of $(Mg,Fe)SiO_3$ in the present P–T conditions generated by experiments with SD anvils.

1. Introduction

High-pressure and temperature generations are the most essential importance in the experimental study of the Earth's interior. In this context, the Kawai-type multianvil apparatus (KMA) has been widely used as well as the diamond anvil cell (DAC) (cf. Ito, 2015). The conspicuous advantages of the KMA over the DAC are the capability to compress a large volume sample, ~1000 times larger than that of DAC, and create a quasi-hydrostatic environment owing to squeezing an octahedral pressure medium by eight cubic anvils (Kawai and Endo, 1970). Moreover, it is possible to keep the specimen in homogeneous and stable conditions at high temperature by adopting an internal heating system. These advantages make it possible to measure the physicochemical properties of the Earth's minerals precisely under high pressure and temperature conditions (e.g., Nishiyama et al., 2004).

In the KMA, the sample is compressed by concentrating the force produced by the hydraulic press to a small area of

* Corresponding author.
E-mail address: dy@misasa.okayama-u.ac.jp (D. Yamazaki).

https://doi.org/10.1016/j.crte.2018.07.004
1631-0713/

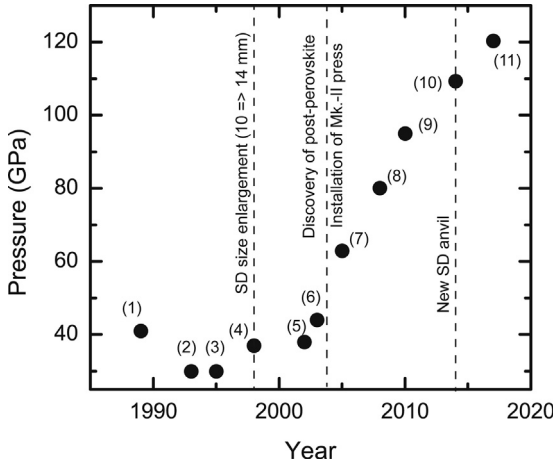

Fig. 1. Evolution of the attainable pressure in the KMA using SD as a second-stage anvil. Data (solid circles) are selected from (1) Ohtani et al. (1989), (2) Kondo et al. (1993), (3) Funamori et al. (1996), (4) Ito et al. (1998), (5) Irifune et al. (2002), (6) Kubo et al. (2003), (7) Ito et al. (2005), (8) Tange et al. (2008), (9) Ito et al. (2010), (10) Yamazaki et al. (2014) and (11) this study.

the sample via cubic anvils. Therefore, the mechanical strength of the anvil material, such as tungsten carbide (WC) and sintered diamond (SD), is key to generating high pressures.

The generated pressure in the KMA with WC anvils had been limited to ~25 GPa (e.g., Keppler and Frost, 2005) for a long time. However, recent development of harder WC material, TJS01 (Fuji Die Co., Ltd.) containing a small amount of Ni binder (< 0.2%), opened a new era to attain pressures much higher than 25 GPa. Kunimoto et al. (2016) generated pressures up to 50 GPa at room temperature, using TJS01 anvils 14 mm in edge length. Later, Ishii et al. (2017) generated pressures up to 65 GPa at room temperature and 48 GPa at 2000 K, using anvils 26 mm in edge length, applying a higher press load.

On the other hand, the attainable pressure with SD anvils has been gradually extended from 1998 to present as shown in Fig. 1. In 1998, SD anvils with a large edge length of 14 mm were introduced, making it possible to apply press loads as high as twice those applied in the previous experiments using 10-mm SD anvils (Ito et al., 1998). The installation of a new DIA-type press (SPEED-Mk.II) (Katsura et al., 2004) enables us to compress the Kawai-type cell more precisely than in experiments using the press installed earlier (SPEED-1500). As a result, the attainable pressure has been extended to ~95 GPa by optimizing the pressure medium and gasket (Ito et al., 2005, 2010; Tange et al., 2008). In our previous study (Yamazaki et al., 2014), we used a new type of SD anvil, "C2-grade", which contains less Co binder of 6–7.5% than the previous type of "C-grade" of 7–8% (Sumitomo Electric Industries, Ltd.). The strength of the "C2-grade"' is slightly higher than that of the "C-grade". The transverse rupture strength (TRS) and Young's modulus of the "C2-grade" are reported to be 1.25 GPa and 940 GPa, respectively, whereas those of the "C-grade" are 1.1 GPa and 920 GPa, respectively (Toda, 2018). Therefore, we could extend the generated pressure to 109 GPa, adopting the "C2-grade" SD anvils.

In this paper, we report on the recent progress of high-pressure generation in the KMA with WC (TJS01) and SD ("C2-grade") anvils with in-situ X-ray diffraction observations for $CaSnO_3$ perovskite and $(Mg,Fe)SiO_3$ bridgmanite using WC and SD anvils, respectively. In the experiments with WC anvils, we focused on obtaining an intense diffraction pattern at high pressure, as well as on generating pressure. In the in-situ X-ray experiments with WC anvils in the KMA, the incident and diffracted X-rays are passed through the gap between anvils (Fig. 2), and hence it is important to keep the gap large enough to acquire the diffraction pattern efficiently. Therefore, in this study, we tested the four types of shapes of WC anvils as described below in details.

2. Experimental procedure

In the experiments using WC anvils (TJS01), we used four types of second-stage "cubic" anvils with an edge length of 14 mm and a truncated edge length of 1.0 mm (Fig. 2): (1) an anvil without any shape-processing (hereafter we call "flat anvil") (Fig. 2B), (2) an anvil with a 12° fan-shaped groove from the truncation corner with a depth of 40 μm on one surface (we will call it hereafter "grooved anvil") (Fig. 2C), (3) an anvil with one tapered surface of 1° (we will call it hereafter "tapered anvil") (Fig. 2D), and (4) an anvil with one "partially" tapered surface of 1° (we will call it hereafter "partially tapered anvil") (Fig. 2E). The main purpose of these different shapes is to acquire diffracted X-ray photons efficiently. Therefore, four anvils of eight cubes composing the Kawai-type cell were shape-processed, and the shape-processed surface was only used to secure the X-ray path (Fig. 2A). The starting material was a powdered mixture of $CaSnO_3$ perovskite, which was synthesized by heating a mixture of $CaCO_3$ and SnO_2 at 1300 K in air for 24 h and Au with a weight ratio of 8:1.

In the experiments using SD anvils, we used 0.3° tapered anvils with a truncated edge length of 1.0 mm and an edge length of 14 mm. Three surfaces of the anvil were tapered for all eight cubes to obtain higher pressure-generation efficiency and to keep the anvil gap large (Fig. 2F and G). For the preparation of the two starting materials, we synthesized $(Mg_{0.9}Fe_{0.1})_2Si_2O_4$-ringwoodite plus Au (6:1 in weight) for run M1626 and $Mg_{0.9}Fe_{0.1}SiO_3$·6 wt % Al_2O_3 bridgmanite plus Au (8:1 in weight) for run M2126 at high pressure and temperature using the KMA at the Institute for Planetary Materials, Okayama University, Japan. After recovery to the ambient condition, the sintered mixtures were shaped into discs 0.4 mm in diameter and 0.3 mm in height to set inside the cylindrical heater.

For the Kawai-type cell in both the WC and SD experiments, we used a small cylindrical TiB_2 + BN + AlN heater put in the MgO + 5% Cr_2O_3 octahedral pressure medium with an edge length of 4.1 mm, and a pyrophyllite gasket baked at 1083 K for 24 min. The low X-ray absorbency of the heater material makes it possible to observe X-ray diffraction of the sample as well as a

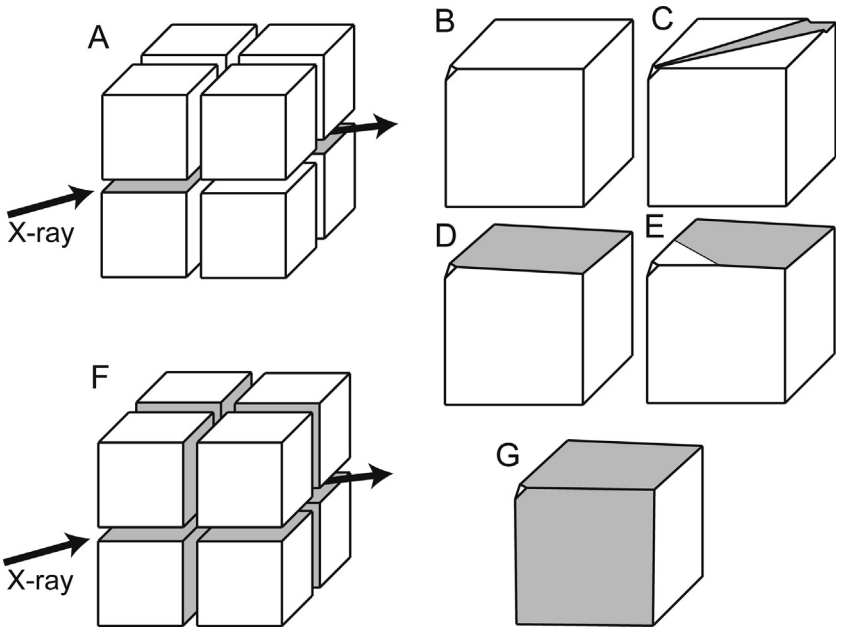

Fig. 2. Schematic drawing of shape-processed cubic anvils. The assemblies of eight cubic anvils for WC and SD anvil experiments are shown in (A) and (F), respectively, where the shaded regions show the shape-processed surfaces. In the experiments with WC anvils, a "flat anvil" (B), a "grooved anvil" (C), a "tapered anvil" (D), and a "partially tapered anvil" were used. In the experiments using SD anvils, only three surface-tapered anvils (G) were used. In (C)–(E) and (G), the shaded regions show the shape-processed region. Arrows indicate the incident and diffracted X-rays.

radiographic image of the sample configuration under compression. The details of cell assembly is shown in Fig. 3, imaged as an X-ray radiography in Fig. 4A and described elsewhere (fig. 2 in Yamazaki et al., 2014). A diamond powder located near the sample may help to generate high pressure in this cell assembly. Temperature was monitored by a $W_{97\%}Re_{3\%}$-$W_{75\%}Re_{25\%}$ thermocouple with a diameter of 0.05 mm. The pressure effect on EMF of the thermocouple was ignored. The pressure was determined from the volume of Au mixed with the sample, based on the equation of state for Au proposed by Tsuchiya (2003).

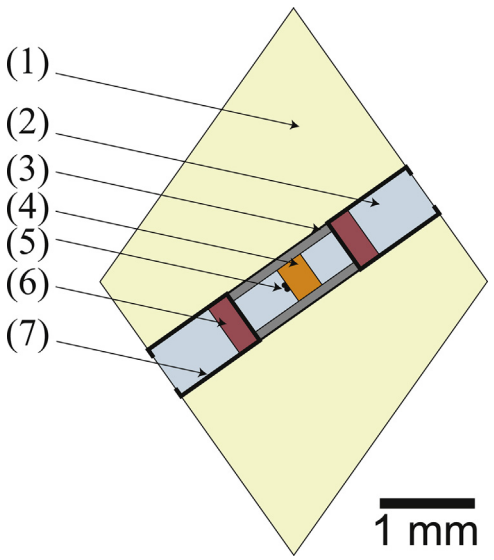

Fig. 3. Schematic drawing of cell assembly which used in the both of experiments with WC and SD anvils. 1: MgO + 5% Cr_2O_3 pressure medium, 2: diamond insulator, 3: TiB_2 + BN + AlN heater, 4: sample, 5: $W_{97\%}Re_{3\%}$-$W_{75\%}Re_{25\%}$ thermocouple, 6: $LaCrO_3$ thermal insulator, 7: Re electrode.

In situ X-ray diffraction experiments at high pressure and temperature were conducted at beamline BL04B1, SPring-8 synchrotron radiation facility using the DIA-type press (SPEED-Mk.II) (Katsura et al., 2004). The energy-dispersive powder X-ray diffraction technique was adopted, with a polychromatic X-ray beam at a diffraction angle of ~6° in conjunction with a germanium solid-state detector. The sample was irradiated by the collimated beam with a size of 50 μm horizontally and 100 μm vertically. A multi-channel analyzer was used to collect the diffracted photons in a range of 20–140 keV through the sandwiched gaskets (anvil gaps). The energies of the photons were calibrated using the characteristic fluorescence X-ray lines of Cu, Mo, Ag, Ta, Pt, Ag, and Pb, or radiation sources of ^{55}Fe, ^{57}Co and ^{133}Ba. The precision in the energy measurements was approximately 30–100 eV per channel. During the acquisition of the diffracted photons, the sample was rotated around the vertical axis between 0° and 6° with respect to the direction of the incident X-ray beam by oscillating the press to average the diffraction profile and to minimize the effect of grain growth (Katsura et al., 2004).

3. Result and discussion

3.1. Pressure generation and observation of $CaSnO_3$ with WC anvils

In the pressure-generation tests, we measured the generated pressure at intervals of 50–100 tons, except for

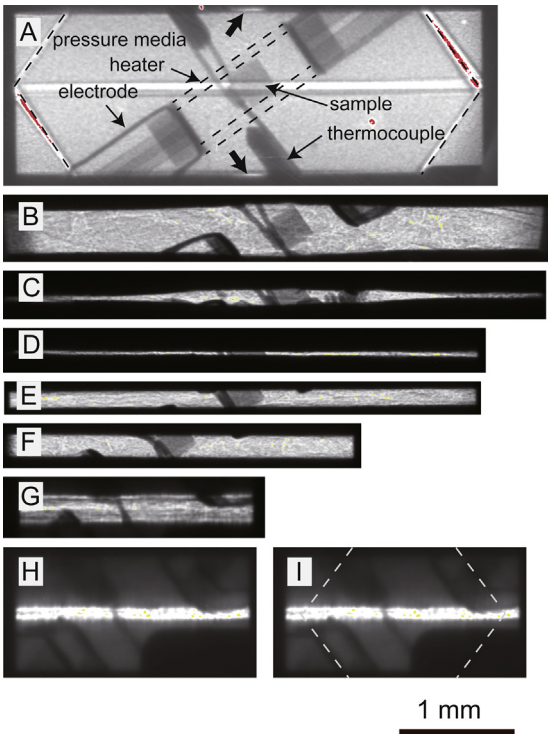

Fig. 4. Images of cell assemblies obtained by X-ray radiography via anvil gaps for the experiments with WC anvils: before compression (A), at 2.0 MN (B) and at 6.5 MN (C) in run M2342 with "grooved anvils", at 6.5 MN in run M2206 with "flat anvil" (D), at 6.5 MN in run M2345 with "partially tapered anvil" (E) and at 6.5 MN in run M2243 with "tapered anvil" (F). Radiographies of the cell assembly in the experiments with SD anvils (run M2126) observed via the anvil gap and the SD anvil at 6.0 MN (G) and 12 MN (H and I) are also shown. In (I), the outline of the pressure medium is guided by broken lines. Thick arrows in (A) indicate the grooves on the anvil surfaces. Note the curved edges of anvil gaps in (B) and (C).

runs M2206 and M2243, in which we directly compressed to higher values than 60 GPa. After compression at room temperature, we heated the sample up to 1500 K in run M2345. We conducted several tests for the pressure generation with WC anvils (Table 1). In Fig. 5, representative results of the pressures generated are shown as a function of the press load using WC anvils. Although we used four types of shape-processed anvils, i.e. "flat anvil" in run M2206, "tapered anvil" in run M2243, "partially tapered anvil" in run M2345, and "grooved anvil" in run M2342, the pressure generation was virtually identical (within ± 5%) up to ~70 GPa, suggesting that shape-processing of only one surface for an anvil and usage of only four shape-processing anvils in KMA (Fig. 2) do not significantly affect pressure generation. In run M2234, the pressure reached 71.3 GPa at a press load of 7.5 MN at room temperature. Pressure-generation efficiency against press load in the present study is higher than that in previous study by Ishii et al. (2017). They used eight 1°-three-surface-tapered anvils, but with a larger truncated edge length of 1.5 mm.

The anvil gap was observed by X-ray radiography (Fig. 4A–F). At 6.5 MN, the anvil gap decreased in the order of the "tapered anvil" (~210 μm, Fig. 4F), "partially tapered anvil" (~150 μm, Fig. 4E), and "flat anvil" (~30 μm, Fig. 4D). The anvil gap with "grooved anvil" in run M2342 (Fig. 4C) was similar to that with "partially tapered anvil" in M2345. Due to the very narrow anvil gap with the "flat anvil" in run M2206, the diffraction intensity was very weak. In run 2342 with "grooved anvil", the horizontal width of the depression in the anvil gap increased with increasing pressure, i.e. ~0.3 mm at ambient pressure (Fig. 4A), ~1.8 mm at 2.0 MN (Fig. 4B) and ~2.7 mm at 6.5 MN (Fig. 4C). Based on this observation, we consider the deformation of anvils under high pressure, i.e. the deformation front on the anvil surface progresses from the center of the Kawai-cell with

Table 1
Experimental conditions and generated pressures.

Run no.	Load (MN)	*P* at RT[a] (GPa)	*T* (K)	*P* at HT[b] (GPa)	Anvil type	Remarks
Experiments with WC anvils						
M2206	6.5	64.7 (0.6)	1400	44.0 (0.4)	"flat"	Blow-out during decompression
M2342	6.5	67.8 (0.2)	1100	52.8 (0.4)	"grooved"	At 6.5 MN, blow-out during increasing temperature at ~1150 K
M2345	6.5	68.4 (0.8)	1500[c] (93)[d]	48.4 (1.0)	"partially tapered"	Blow-out during decompression
M2243	7.5	71.3 (0.3)	300	n.d.[e]	"tapered"	At 7.5 MN, blow out at ~1500 K during increasing temperature
Experiments with SD anvils						
M1626	8.0	112.7 (0.2)	300	n.d.[e]	Three surface-tapered	At 8.0 MN, blow out at ~600 K during increasing temperature
M2126	13.0	120.3 (0.2)	1673[c] (92)[f]	105.0 (0.9)	Three surface-tapered	Blow-out during decompression

Numbers in parentheses represent the uncertainties of pressures.
[a] The highest pressure at room temperature.
[b] Pressure at high temperature.
[c] Temperature was estimated from the input power because of thermocouple failure.
[d] The uncertainty of temperature is derived from the reproducibility of power-temperature relation in the other runs.
[e] Not determined.
[f] The uncertainty of temperature is derived from the uncertainty of extrapolation of power-temperature relation at the lower pressure.

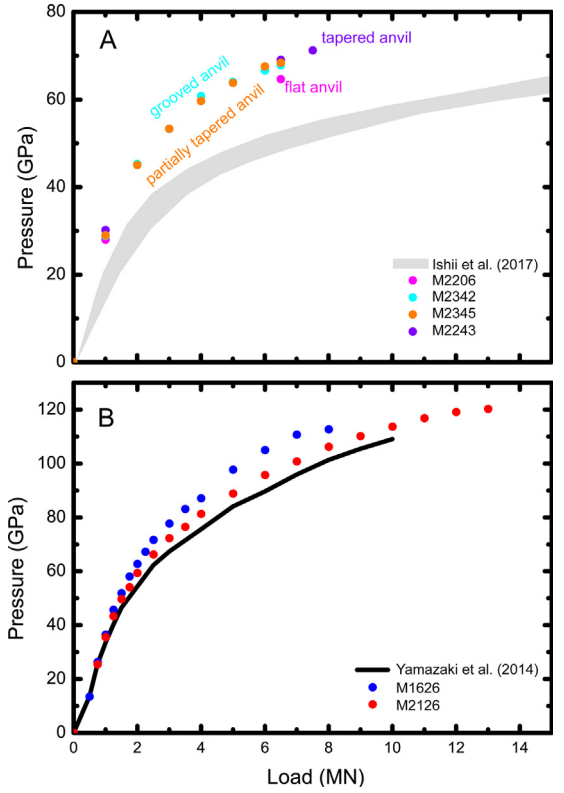

Fig. 5. Generated pressures versus the press load in runs equipped with WC (A) and SD anvils (B). In runs M1626 and M2126, pressure was measured after annealing, whereas pressure at 8.0 MN in run M1626 was measured before annealing. Data in runs M2206, M2243, M2342 and M2345 were obtained during compression at room temperature.

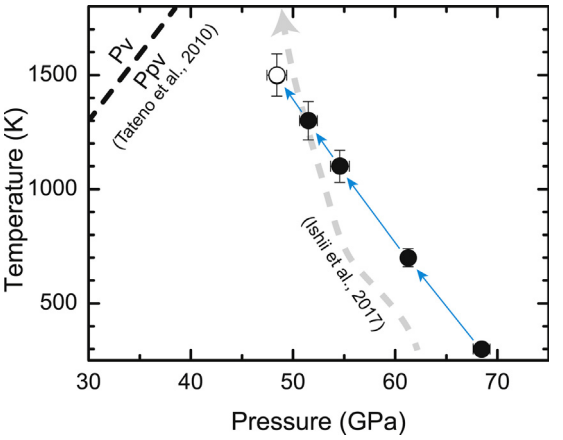

Fig. 6. Pressure reduction on heating up to 1500 K in run M2345, together with earlier data by Ishii et al. (2017). The dashed line shows the phase boundary between perovskite and post-perovskite in $CaSnO_3$ determined in the DAC experiment (Tateno et al., 2010), in which the Pt pressure scale (Holmes et al., 1989) was adopted. Solid and open symbols represent the *P–T* conditions where only perovskite peaks were observed, and perovskite peaks with new small peaks were observed (as shown in Fig. 7), respectively.

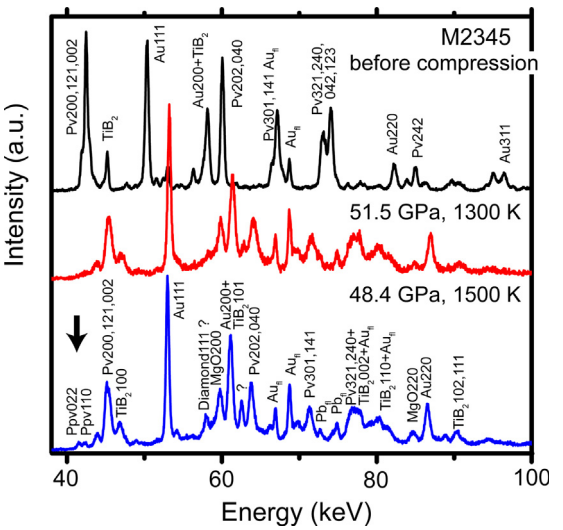

Fig. 7. Representative X-ray diffraction patterns of $CaSnO_3$ perovskite mixed with gold at a press load of 6.5 MN (run M2345). Note that there are new small peaks at 48.4 GPa and 1500 K, indicated by an arrow.

increasing pressure. The deformation front at 6.5 MN is estimated to be ~13 mm away from the center because of a totally 12° fan-shaped groove. The value of ~13 mm is considered to be much larger than the flow length of gasket (~7 mm) at 6.5 MN in the present study. Therefore, it is likely that the plastic deformation of anvils caused by the compression of the gasket is limited over the area near the truncation corner, whereas the elastic deformation occurs over the larger area of the anvil's surface.

In run M2345, we heated the sample of $CaSnO_3$ perovskite along the path shown in Fig. 6. With increasing temperature, the pressure almost linearly decreased from 68.4 ± 0.8 GPa at 300 K to 48.4 ± 1.0 GPa at 1500 ± 93 K (Table 1). The drop of ~20 GPa in this study is larger than that in the previous study (Ishii et al., 2017) presumably due to smaller cell assembly and lower press load in the present study. Fig. 7 shows the representative diffraction patterns acquired at ambient and at high pressure and temperature conditions. In comparison with diffraction peaks at ambient pressure, the broad peaks indexed as only perovskite were observed even at 1300 K. By subsequent heating to 1500 K, however, new small peaks appeared. Based on the previous DAC experiment on phase boundary between perovskite and post-perovskite in $CaSnO_3$ (Tateno et al., 2010), it seems that these peaks are likely to be from the intense (022) and (110) peaks of the post-perovskite phase. However, these small peaks did not grow for 30 min at 1500 K after their appearance, suggesting slow kinetics of transformation into $CaSnO_3$ consistent with previous studies of the perovskite-to-post-perovskite transformation in silicates (e.g., Dorfman et al., 2013). By subsequently heating to higher temperature, the intensity of diffraction pattern became weak and the heater finally failed. As a conclusion, we could not resolve post-perovskite peaks clearly. In order to observe the post-perovskite phase more definitely, experiments at higher pressure and temperature are required.

3.2. Pressure generation and observation of $(Mg,Fe)SiO_3$ with SD anvils

During compression, we annealed the sample at every 5–10 GPa interval up to 800–1000 K to relax stress and to reduce the probability of explosion of the specimen (i.e. so called "blow out"). Representative results of pressure generation with SD anvils versus the press load are shown in Fig. 5 (M1626 and 2126), in which pressures were determined after annealing at 800–1000 K, except for the pressure at 8.0 MN in run M1626. The pressure reached 112.7 GPa at 8.0 MN and 300 K before annealing in run M1626 (Table 1). Although the pressure-generation efficiency of this run is higher than the previous results shown in the solid line in Fig. 5 due to the usage of smaller gaskets, the run was terminated by blow-out while increasing temperature up to ~550 K. In run M2126, we successfully increased the press load up to 13.0 MN despite the use of 14-mm-edge-length anvils because of the harder first-stage anvil with the transverse rupture strength (TRS) of 4410 MPa (F09 grade, Fuji Die Co., Ltd.). In the previous study (Yamazaki et al., 2014), we used more brittle materials for the first-stage anvil (F10 grade, Fuji Die Co., Ltd.) with TRS = 3820 MPa and the maximum press load was limited to ~10 MN. As a result, in this study the pressure reached 120.3 GPa at room temperature after annealing at 760 K, although the generation efficiency in this run was lower than that in M1626 and was virtually identical (within ± 5%) to that in the previous experiment (Yamazaki et al., 2014).

As mentioned previously, the wide anvil gap is favorable to acquiring the diffracted X-rays. In run M2126, the anvil gap at 6.0 MN was wider than the vertical size of the incident X-ray beam of 100 μm (Fig. 4G). This anvil gap was also larger than the anvil gap in the experiment with a WC anvil, even if the taper angle was smaller in SD anvils (Fig. 4F), suggesting a smaller deformation of the SD anvils with respect to that of the WC anvils. At 13.0 MN, the anvil gap was less than 100 μm, and hence the intensity of the diffracted X-ray was less than a half of that at 6.0 MN, as shown in Fig. 8. Although we obtained an X-ray pattern sufficient to determine the pressure using Au peaks and to identify the phases present, a more intense X-ray pattern is required to determine lattice constants of the sample precisely. Observation of the cell assembly through the SD anvil by radiography (Fig. 4H) showed that the edge length of the octahedral space is estimated to be ~1.2 mm at 12.0 MN, indicating a gasket thickness of ~0.4 mm that is much larger than the apparent anvil gap of ~80 μm. This discrepancy shows a large deformation of the anvil at high pressure, even with SD. Because the plastic deformation of the anvil surface is negligibly small, as one can judge from the observation of the recovered SD anvils, elastic deformation dominates the total deformation of the anvil at high pressure.

In M2126, we re-heated the sample up to 760 ± 30 K and kept the temperature constant for 30 min at 120.4 ± 0.4 GPa (Table 1). Under these conditions, the diffraction peaks can be assigned to bridgmanite although the *P–T* conditions seem to be in the stability field of post-perovskite, inferred from DAC experiments (Tateno et al., 2009) (Fig. 9). This indicates that the temperature is too low to enhance the phase transformation to the post-perovskite phase due to slow kinetics (e.g., Dorfman et al., 2013). The subsequent heating to 1673 ± 92 K caused a conspicuous pressure drop to 105.0 ± 0.9 GPa (Table 1), because annealing temperatures of less than 1000 K during compression were much lower than 1673 K, which might be out of the stability field of post-perovskite. In the present study, thus, we could not observe the silicate post-perovskite phase.

The attainable pressure with the Kawai-type apparatus equipped with SD anvils has reached ~120 GPa, corresponding to the depth of the D" layer in the Earth's mantle, due to the developments motivated by the discovery of post-perovskite (Murakami et al., 2004). However, more improvements of the cell assembly are necessary, including adopting more effective thermal insulation to allow us

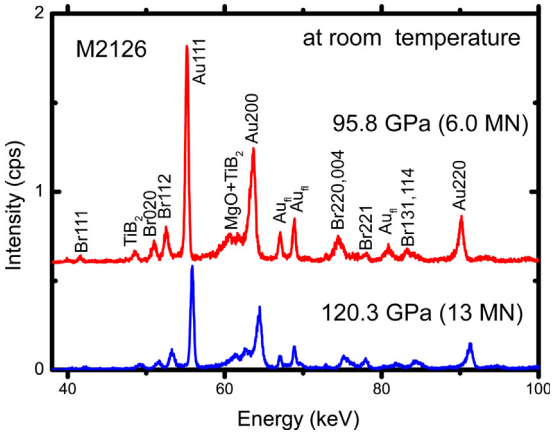

Fig. 8. Representative diffraction profiles $Mg_{0.9}Fe_{0.1}SiO_3$ + 6 wt % Al_2O_3 bridgmanite mixed with gold at 95.8 GPa and 120.3 GPa at room temperature after annealing in run M2126. Intensity is normalized by the acquisition time.

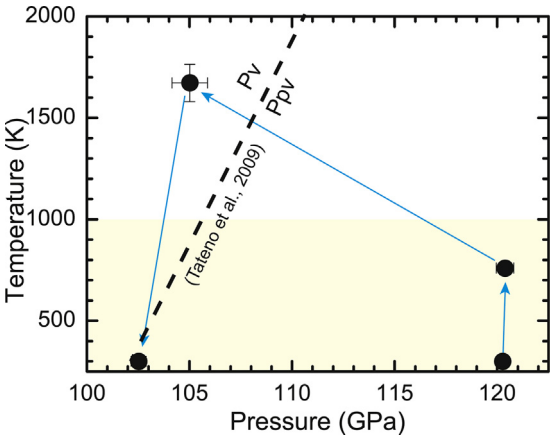

Fig. 9. *P–T* path in run M2126, showing the attainable pressure and the temperature range in the KMA over ~100 GPa. The dashed line shows the estimated phase boundary between bridgmanite and post-perovskite in $MgSiO_3$ by the extrapolation of the results in the DAC experiment (Tateno et al., 2009), in which the Au pressure scale (Tsuchiya, 2003) was used. The yellow-color region displays the temperature for annealing during compression.

to generate higher temperatures and to reduce the possibility of blow out, which frequently occurs during heating. Al_2O_3 may be a more effective pressure medium than the Cr-doped MgO used in the present study (Tange et al., 2008), and boron-doped diamond may be usable to generate high temperature over 2000 K (Shatskiy et al., 2009). Furthermore, in order to generate higher pressure, the development of an SD material, i.e. with a higher hardness and a larger size, is most crucial. The highest pressure of 120 GPa was obtained by compression until 13.0 MN in this study, and the larger size of the SD anvils may enable us to apply a large press load ($>$ 13.0 MN) routinely. The high-quality harder SD reduces the deformation of anvils at high pressure and enables a better acquisition of the diffracted X-rays as well as the generation of higher pressures. In addition to the development of SD anvils, binderless sintered diamonds such as nano-polycrystalline diamond (Irifune et al., 2003) and nano-twinned diamond (Huang et al., 2014) are good candidates for being the anvil material of the next generation in the KMA.

Acknowledgements

We thank C. Oka for experimental supports, M. Izawa for reading the manuscript, and anonymous reviewers for valuable comments. X-ray diffraction measurements were conducted at BL04B1, SPring-8, Japan (proposal Nos. 2014A1737, 2014B1424, 2015A1913, 2015B1319, 2016A1716, 2016B1486, 2017A1740, 2017B1324).

References

Dorfman, S.M., Meng, Y., Prakapenka, V.B., Duffy, T.S., 2013. Effects of Fe-enrichment on the equation of state and stability of $(Mg,Fe)SiO_3$ perovskite. Earth Planet. Sci. Lett. 361, 249–257.

Funamori, N., Yagi, T., Utsumi, W., Kondo, T., Uchida, T., Funamori, M., 1996. Thermoelastic properties of $MgSiO_3$ perovskite determined by in situ X ray observations up to 30 GPa and 2000 K. J. Geophys. Res. 101, 8257–8269.

Holmes, N.V., Moriarty, J.A., Gathers, G.R., Nellis, W.J., 1989. The equation of state of platinum to 660 GPa (6.6 Mbar). J. Appl. Phys. 66, 2962–2967.

Huang, Q., Yu, D., Xu, B., Hu, W., Ma, Y., Wang, Y., Zhao, Z., Wen, B., He, J., Liu, Z., Tian, Y., 2014. Nanotwinned diamond with unprecedented hardness and stability. Nature 540, 250–253.

Irifune, T., Naka, H., Sanehira, T., Inoue, T., Funakoshi, K., 2002. In situ X-ray observations of phase transitions in $MgAl_2O_4$ spinel to 40 GPa using multianvil apparatus with sintered diamond anvils. Phys. Chem. Miner. 29, 645–654.

Irifune, T., Kurio, A., Sakamoto, S., Inoue, T., Sumiya, H., 2003. Ultrahard polycrystalline diamond from graphite. Nature 421, 599–600.

Ishii, T., Yamazaki, D., Tsujino, N., Fang, X., Liu, Z., Kawazoe, T., Yamamoto, T., Druzhbin, D., Wang, L., Higo, Y., Tange, Y., Yoshino, T., Katsura, T., 2017. Pressure generation to 65 GPa in Kawai-type multi-anvil apparatus with tungsten carbide anvils. High Press. Res. 37, 507–515.

Ito, E., 2015. Theory and practice-multianvil cells and high-pressure experimental methods. In: Schubert, G., Romanowicz, B., Dziewonski, A. (Eds.), Treatise on Geophysics, Second edition: Mineral Physics. pp. 233–261.

Ito, E., Kubo, A., Katsura, T., Akaogi, M., Fujita, T., 1998. High-pressure transformation of pyrope $(Mg_3Al_2Si_3O_{12})$ in a sintered diamond cubic anvil assembly. Geophys. Res. Lett. 25, 821–824.

Ito, E., Katsura, T., Aizawa, Y., Kawabe, K., Yokoshi, S., Kubo, A., Nozawa, A., Funakoshi, K., 2005. High-pressure generation in the Kawai-type apparatus equipped with sintered diamond anvils: application to the wurtzite-rocksalt transformation in GaN. In: Chen, J., Wang, Y., Duffy, T.S., Shen, G., Dobrzhinetskaya, L.F. (Eds.), Advances in High-Pressure Technology for Geophysical Applications. Elsevier, Amsterdam, pp. 451–460.

Ito, E., Yamazaki, D., Yoshino, T., Fukui, H., Zhai, S., Shatzkiy, A., Katsura, T., Tange, Y., Funakoshi, K., 2010. Pressure generation and investigation of the post-perovskite transformation in $MgGeO_3$ by squeezing the Kawai-cell equipped with sintered diamond anvils. Earth Planet. Sci. Lett. 293, 84–89.

Katsura, T., Funakoshi, K., Kubo, A., Nishiyama, N., Tange, Y., Sueda, Y., Kubo, T., Utsumi, W., 2004. A large-volume high P–T apparatus for in situ X-ray observation, 'SPEEDMkII'. Phys. Earth Planet Inter. 143–144, 497–506.

Kawai, N., Endo, S., 1970. The generation of ultrahigh hydrostatic pressure by a split sphere apparatus. Rev. Sci. Instrum. 4, 425–428.

Keppler, H., Frost, D., 2005. Introduction to minerals under extreme conditions. In: Miletich, R. (Ed.), Mineral Behavior at Extreme Conditions. Eötvös University Press, Budapest, pp. 1–30.

Kondo, T., Sawamoto, H., Yoneda, A., Kato, M., Matsumoto, A., Yagi, T., 1993. Ultrahigh-pressure and high-temperature generation by use of the MA8 system with sintered-diamond anvils. High Temp.–High Press. 25, 105–112.

Kubo, A., Ito, E., Katsura, T., Shinmei, T., Yamada, H., Nishikawa, O., Song, M., Funakoshi, K., 2003. In situ X-ray observation of iron using Kawai-type apparatus equipped with sintered diamond: Absence of β phase up to 44 GPa and 2100 K. Geophys. Res. Lett. 30 , http://dx.doi.org/10.1029/2002GL016394.

Kunimoto, T., Irifune, T., Tange, Y., Wada, K., 2016. Pressure generation to 50 GPa in Kawai-type multianvil apparatus using newly developed tungsten carbide anvils. High Press Res. 36, 1–8.

Murakami, M., Hirose, K., Kawamura, K., Sata, N., Ohishi, Y., 2004. Post-perovskite transition in $MgSiO_3$. Science 304, 855–858.

Nishiyama, N., Irifune, T., Inoue, T., Ando, J., Funakoshi, K., 2004. Precise determination of phase relations in pyrolite across the 660 km seismic discontinuity by in situ X-ray diffraction and quench experiments. Phys. Earth Planet. Int. 143–144, 185–199.

Ohtani, E., Kagawa, K., Shimomura, O., Togaya, M., Suito, K., Onodera, A., Swamoto, H., Yoneda, A., Utsumi, W., Ito, E., Wakatsuki, A., Kikegawa, T., 1989. High-pressure generation by a multiple anvil system with sintered diamond anvils. Rev. Sci. Instrum. 60, 922–925.

Shatskiy, A., Yamazaki, D., Morard, G., Cooray, T., Matsuzaki, T., Higo, Y., Funakoshi, K., Sumiya, H., Ito, E., Katsura, T., 2009. Boron-doped diamond heater and its application to large-volume, high-pressure, and high-temperature experiments. Rev. Sci. Instrum. 80, 023907.

Tange, Y., Irifune, T., Funakoshi, K., 2008. Pressure generation to 80 GPa using multianvil apparatus with sintered diamond anvils. High Press. Res. 28, 245–254.

Tateno, S., Hirose, K., Sata, N., Ohishi, Y., 2009. Determination of post-perovskite phase transition boundary up to 4400 K and implications for thermal structure in D″ layer. Earth Planet. Sci. Lett. 277, 130–136.

Tateno, S., Hirose, K., Sata, N., Ohishi, Y., 2010. Structural distortion of $CaSnO_3$ perovskite under pressure and quenchable post-perovskite phase as a low-pressure analogue to $MgSiO_3$. Phys. Earth Planet. Int. 181, 54–59.

Toda, N., 2018. Polycrystalline diamond sintered materials used in high pressure science. Rev. High Press. Sci. Technol. 28, 23–27 (in Japanese with English abstract).

Tsuchiya, T., 2003. First-principles prediction of the P-V-T equation of state of gold and the 660-km discontinuity in Earth's mantle. J. Geophys. Res. 108 , http://dx.doi.org/10.1029/2003JB002446.

Yamazaki, D., Ito, E., Yoshino, T., Tsujino, N., Yoneda, A., Guo, X., Xu, F., Higo, Y., Funakoshi, K., 2014. Over 1Mbar generation in the Kawai-type multianvil apparatus and its application to compression of $(Mg_{0.92}Fe_{0.08})SiO_3$ perovskite and stishovite. Phys Earth Planet Inter. 228, 262–267.